On the Bound Wave Phase Lag

Thomas Guérin [1],*[ID]**, Anouk de Bakker** [2] **and Xavier Bertin** [3]

1   SAS Benoit Waeles–Consultant Génie Côtier, 53 rue du Commandant Groix, 29200 Brest, France
2   Unit of Marine and Coastal Systems, Deltares, 2600 Delft, The Netherlands
3   UMR 7266 LIENSs CNRS-Université de La Rochelle, 2 rue Olympe de Gouges, 17000 La Rochelle, France
*   Correspondence: thomas.guerin@bw-cgc.fr

Abstract: More than three decades ago, it was noted that the ocean infragravity bound wave increasingly lags behind the forcing short-wave groups when propagating towards the shore. To date, the most recent theoretical prediction of this so-called phase lag remained a first-order approximation in terms of depth variations. Here, a new semi-analytical solution is proposed which does not rely on this approximation. Strong agreement is obtained when the new solution is compared with high-resolution laboratory data involving both bichromatic and random wave conditions. This newly proposed theoretical phase lag is then extensively compared with the former one, highlighting an increasing discrepancy between the two solutions as the relative bottom slope increases. The four influencing parameters, namely the bottom slope, the water depth, the incident short-wave peak period and the incident group period, are shown to impact, each in a specific way, the bound wave phase lag. While the latter is seen to increase with lower water depths and/or with higher short-wave peak periods, both the bottom slope and the group period can affect the phase lag in a different manner. Indeed, steeper bed slopes induce lower phase lags in shallow water but higher ones in deep water, while higher group periods induce higher phase lags for gentle slopes but lower ones for steep slopes.

Keywords: infragravity wave; bound wave; phase lag; GLOBEX; coastal hydrodynamics

---

1. Introduction

Infragravity (IG) waves are ocean surface waves with frequencies typically ranging from 0.004 to 0.04 Hz. Munk [1] and Tucker [2] initially named them "surf beats" when they reported low-frequency oscillations of the sea surface associated with the presence of short-wave groups. Since the observation that these long waves can be quite energetic when reaching the shoreline (e.g., [3,4]), their study became increasingly popular among the coastal community. The phenomenon of harbour resonance induced by the presence of IG waves also contributed to their growing interest (e.g., [5–7]), in view of the potential severe damages involved. The substantial role of IG waves in nearshore hydrodynamics, sediment transport, or even dune and barrier breaching is now well confirmed by field and laboratory experiments, as well as numerical modeling studies (see Bertin et al. [8] for a recent review).

The first theoretical demonstration of the existence of IG waves was the one of Biésel [9], which shows that a modulation of the short-wave amplitude within a wave group causes the mean water level to be lower (respectively, higher) where the short waves are higher (respectively, lower). The low-frequency wave thereby created has the same period as the short-wave group. While also considering a constant water depth, but applying the concept of radiation stress, Longuet-Higgins and Stewart [10] obtained a similar depression of the mean water level under higher short-waves that they interpreted as a consequence of the negative mass-transport tending to expel the fluid from there. The term "bound wave" (or "group-forced long wave") was then associated to this second-order oscillation of the water surface.

Later on, Symonds et al. [11] proposed a model for the generation of IG waves due to the presence of a time-varying breakpoint only (i.e., without considering the short-wave groups outside the surf zone). The so-called (moving) breakpoint mechanism is based on the cross-shore variation of the depth-limited short-wave breaking, due to the difference in short-wave height within the group (i.e., smaller waves break closer to shore than higher waves). Using the depth-integrated, linearized shallow water equations without any forcing effects outside the surf zone, Symonds et al. [11] obtained free wave solutions consisting in standing and progressive IG waves respectively, shoreward and seaward of the breaking zone.

The first consistent theoretical model accounting for both the bound wave and the moving breakpoint mechanism was then developed by Schäffer [12] for a uniform bed slope. In his work, the linearized form of the shallow water equations with a forcing term are fully solved. A different approach was used by Bowers [13] and van Leeuwen [14] (i.e., a perturbation method) to only focus on the bound wave and analytically study how it is affected by the depth gradient. They showed that the phase difference between the bound wave and its forcing shifts away from π radians as the water depth decreases. This result supported the observations of Mansard and Barthel [15] and Elgar and Guza [16] that group-forced long waves were increasingly lagging behind the short-wave envelope when propagating towards the shore. van Dongeren and Svendsen [17] then pinpointed the potential implications of this phase difference by showing how it is related to the work term in the energy equation of the long waves (i.e., the term which includes the radiation stress gradient), and therefore affects the growth rate of the IG wave in the nearshore. This key role regarding the transfer of energy between the short-wave groups and the bound wave was eventually further analyzed by Battjes et al. [18]. Interestingly, an analogous link between energy transfer and phase difference within spectral wave components, also associated with a growth in wave amplitude, has been demonstrated in optics through the study of amplifying laser pulses [19,20].

Since the relevance of this so-called phase lag (or phase shift) between the short-wave envelope and the bound wave was noticed, the work of Janssen et al. [21] (hereafter J03) is to our knowledge the only one to propose a solution for the evolution of this bound wave phase lag over a sloping bottom. One must mention that Nielsen [22] investigated this long wave characteristic (for a single short-wave pulse), but despite the attempt to provide an intuitive understanding of the underlying physical mechanism, the associated approach remains inherently based on the constant-depth solution of the problem while no expression is proposed for actually predicting the phase lag. Similar to the work of van Leeuwen [14], J03 used a perturbation method to propose a linear model accurate to first order in bottom slope for the evolution of the bound wave phase lag. The main progress compared to the approach of van Leeuwen [14] was the ability to include the spatial variation of the long wave amplitude in their theoretical model. They proposed two separate solutions for the phase lag, depending on a parameter which quantifies the departure from a resonant situation and thereby specifying an "off-resonant" and "near-resonant" case. While in their study the near-resonant solution agrees qualitatively well with observations from the laboratory experiments of Boers [23], the fact that it remains a first-order approximation in terms of the bed slope fosters new work on this topic.

The purpose of the present paper is twofold. Firstly, it provides a semi-analytical expression of the bound wave phase lag directly derived from the pioneer work of Schäffer [12], since the latter furnishes the exact solution to the linearized shallow-water equations (with a forcing term) suiting to the problem of group-forced long waves propagating over a sloping bottom. Secondly, it broadens the range of comparisons between theoretical and observed phase lags, while considering both our new solution and the ones of J03 on the theoretical side. Section 2 summarizes the approach of Schäffer [12] and presents the analytical derivation of the phase lag solution. Comparisons with data from the GLOBEX laboratory experiments [24] are analyzed in Section 3. The predicted behavior of the bound wave phase lag is then broadly investigated in Section 4, through an inter-comparison of the two relevant theoretical solutions. Conclusions are given in Section 5.

2. Mathematical Model

2.1. Theoretical Framework

The governing equation solved by Schäffer [12] for a uniform beach slope and a 1DH situation is the linearized shallow-water equation with a forcing term:

$$\frac{\partial}{\partial x}\left(gh\frac{\partial \eta_1}{\partial x}\right) - \frac{\partial^2 \eta_1}{\partial t^2} = -\frac{1}{\rho}\frac{\partial^2 S_{xx,1}}{\partial x^2} \tag{1}$$

where x is the horizontal coordinate (vanishing at the shoreline and positive seaward), t is the temporal coordinate, g is the gravitational acceleration, ρ is the water density, and $h = xh_x$ is the water depth where h_x is the constant bed slope. $\eta_1(x,t)$ is the elevation of the IG wave component, while $S_{xx,1}(x,t)$ is the radiation stress forcing associated with the IG angular frequency $\omega_g = 2\pi/T_g$, where T_g is the short-wave group period. The computation of $S_{xx,1}$ follows:

$$S_{xx,1} = S_{xx} - S_{xx,0} = \rho g \left(A^2 - a^2\right)\left(\frac{c_g}{c} - \frac{1}{4}\right) \tag{2}$$

where $S_{xx,0}(x)$ is the temporal mean (or group-averaged value) of the total radiation stress term $S_{xx}(x,t)$, $A(x,t)$ is the amplitude of the short-wave envelope and $a(x)$ is its temporal mean, c is the phase velocity of the short waves, and c_g is the group velocity. The usual law of conservative shoaling for linear waves is considered to describe the cross-shore evolution of the short-wave amplitude outside the surf zone:

$$a^2 = \frac{c_{g,off}}{c_g}\,a_{off}^2 \tag{3}$$

where the subscript off refers to the offshore boundary value. The short-wave amplitude in the surf zone is proportional to the local water depth, which is commonly written $a = \gamma_b h$ with γ_b being the breaker index.

One can note that the so-called long-wave Equation (1) was already the one solved by Longuet-Higgins and Stewart [10] in the particular case of a constant depth and resulting in the equilibrium bound wave being exactly π out of phase with the short-wave envelope and thus travelling at the wave group velocity. In this approach, the general solution of this equation is obtained by considering only harmonic solutions, allowing to write both the surface elevation and the radiation stress using Fourier series, and thus removing the time variable of the problem. Equation (1) then becomes the following ordinary differential equation:

$$\frac{d}{dx}\left(gh\frac{d\xi_1}{dx}\right) + \omega_g^2 \xi_1 = -\frac{1}{\rho}\frac{d^2 S_1}{dx^2} \tag{4}$$

where $\xi_1(x)$ and $S_1(x)$ are the spatial part of the group-frequency surface elevation and radiation stress, respectively.

By performing an appropriate change of variable and using the method of variations of parameters, the solution to Equation (4) can be written (using the real representation) as:

$$\xi_1 = J_0\left(\alpha_1 + \int_{x_l}^{x}\frac{-Y_0\,\mathbb{S}_1}{W}dx\right) + Y_0\left(\beta_1 + \int_{x_l}^{x}\frac{J_0\,\mathbb{S}_1}{W}dx\right) \tag{5}$$

where the zeroth-order Bessel functions of first and second kind, $J_0(X)$ and $Y_0(X)$, are the homogeneous solutions depending on the dimensionless variable $X = 2\omega_g\sqrt{x/(gh_x)}$, $W(X)$ is their Wronskian, x_l is the lower limit of integration, and α_1 and β_1 are two integration constants (see Section 4.2.3 of

Schäffer [12] for the determination procedure of these constants). $\mathbb{S}_1(x)$ corresponds to the forcing term (i.e., right-hand side of the normalized equation) and reads:

$$\mathbb{S}_1 = -\frac{1}{\rho g h} \frac{d^2 S_1}{dx^2} \tag{6}$$

Because the present paper focuses on the infragravity bound wave only, the specific case of no reflection at the shoreline is considered here (i.e., no free waves propagating seaward) along with a fixed breakpoint position which avoids the presence of breakpoint-generated free waves. This particular configuration is considered in Section 4.3.2 of the work of Schäffer [12] which thus constitutes our benchmark to ensure the correct computation of the associated solution (see Appendix A).

2.2. Derivation of the Bound Wave Phase Lag

In the present paper, the bound wave phase lag $\phi_{lag}(x)$ is defined as the phase difference between the crest (respectively, the trough) of the short-wave envelope and the trough (respectively, the crest) of the bound wave, meaning that we consider $\phi_{lag} = 0$ for the anti-phase situation (i.e., the equilibrium solution of Longuet-Higgins and Stewart [10]).

One way to reach an expression of the phase lag is to compare the cross-shore evolution of the vanishing forcing locations (i.e., x-coordinates) with the vanishing infragravity wave locations. Mathematically, it consists in comparing the solutions of $S_1(x) = 0$ and $\zeta_1(x) = 0$. Note that this approach is straightforward compared to the approach of finding the locations of maximum (or minimum) forcing and response, the latter requiring to consider a vanishing derivative.

For the forcing, sticking to the notation of Schäffer [12] (i.e., Equation (4.20) in his work), the vanishing condition leads to:

$$S_1 = \rho g \, a^2 \, 2\delta \cos\left(\int_{x_l}^{x} \frac{\omega_g}{c_g} dx\right) \left(\frac{c_g}{c} - \frac{1}{4}\right) = 0 \tag{7}$$

where δ is the amplitude modulation. Since only the cosine term can vanish, Equation (7) is equivalent to:

$$\int_{x_l}^{x} \frac{\omega_g}{c_g} dx - \frac{\pi}{2} \equiv 0 \pmod{\pi} \tag{8}$$

Now, considering the vanishing infragravity response, we have:

$$\zeta_1 = J_0 \left(\alpha_1 + \int_{x_l}^{x} \frac{Y_0}{W} \frac{1}{\rho g h} \frac{d^2 S_1}{dx^2} dx\right) + Y_0 \left(\beta_1 - \int_{x_l}^{x} \frac{J_0}{W} \frac{1}{\rho g h} \frac{d^2 S_1}{dx^2} dx\right) = 0 \tag{9}$$

By using the asymptotic expansions of the Bessel functions for large arguments (see Sections 9.2.1–9.2.2 of Abramowitz et al. [25]), and $W = 1/(\pi x)$ (see Equation (4.36) of Schäffer [12]), Equation (9) transforms to:

$$\sqrt{\frac{2}{\pi X}} \cos\left(X - \frac{\pi}{4}\right) \left(\alpha_1 + \int_{x_l}^{x} \sqrt{\frac{2\pi}{X}} \sin\left(X - \frac{\pi}{4}\right) \frac{1}{\rho g h_x} \frac{d^2 S_1}{dx^2} dx\right) \tag{10}$$

$$+ \sqrt{\frac{2}{\pi X}} \sin\left(X - \frac{\pi}{4}\right) \left(\beta_1 - \int_{x_l}^{x} \sqrt{\frac{2\pi}{X}} \cos\left(X - \frac{\pi}{4}\right) \frac{1}{\rho g h_x} \frac{d^2 S_1}{dx^2} dx\right) = 0 \tag{11}$$

which leads to:

$$\tan\left(X - \frac{\pi}{4}\right) = \left(\frac{\alpha_1 + \int_{x_l}^{x} F_s \, dx}{-\beta_1 + \int_{x_l}^{x} F_c \, dx}\right) \tag{12}$$

where

$$F_{\{c,s\}} = \sqrt{\frac{2\pi}{X}} \{\cos, \sin\} \left(X - \frac{\pi}{4}\right) \frac{1}{\rho g h_x} \frac{d^2 S_1}{dx^2} \tag{13}$$

We then reach:

$$X - \frac{\pi}{4} - \arctan(\mathbb{F}) \equiv 0 \quad (\text{mod } \pi) \tag{14}$$

with

$$\mathbb{F} = \frac{\alpha_1 + \int_{x_l}^{x} F_s \, dx}{-\beta_1 + \int_{x_l}^{x} F_c \, dx} \tag{15}$$

Since Equations (8) and (14) correspond, respectively, to the spatial part of the phase function of the forcing on the one hand and of the infragravity response on the other hand, the phase lag between both is obtained following two steps. First, the phase difference $\Delta\phi$ is computed by making the difference between the two mentioned expressions:

$$\Delta\phi \equiv \int_{x_l}^{x} \frac{\omega_g}{c_g} dx - \frac{\pi}{4} - 2\omega_g \sqrt{\frac{x}{g h_x}} + \arctan(\mathbb{F}) \quad (\text{mod } \pi) \tag{16}$$

Second, because this phase difference is related to the x-coordinates of the vanishing forcing $S_1(x)$ and thus depends on the arbitrarily-defined lower limit of integration x_l (i.e., different x_l will give different x-coordinates of vanishing S_1), it is necessary to average $\Delta\phi$ over the forcing phase function to obtain the bound wave phase lag (ϕ_{lag}). More precisely, a range of phases is considered for the computation of $\Delta\phi$, i.e., considering $\int_{x_l}^{x} \frac{\omega_g}{c_g} dx + d\theta$ with $d\theta$ ranging from 0 to $(2\pi - d\theta)$, providing a range of phase difference $\Delta\phi(d\theta)$ which is then averaged. This averaging procedure is thus equivalent to remove the dependence of the result on x_l. We eventually use the notation:

$$\phi_{lag} = \langle \Delta\phi \rangle_{2\pi} \tag{17}$$

3. Comparisons between Theory and GLOBEX Laboratory Data

3.1. Experimental Set-Up

The Gently sLOping Beach EXperiments (GLOBEX) were performed in the Scheldt flume of Deltares (Delft, the Netherlands) in 2012, and are extensively described in Ruessink et al. [24]. The flume was 100 m long, with as experimental setup a horizontal part with 85 cm water depth at the wave maker, followed by a fixed beach slope of 1:80 over the other 85% of the flume. To avoid re-reflection of waves at the wave maker, an active reflection compensation was used. Sea-surface elevation measurements were taken at 190 locations (obtained by relocating most of the 21 wave gauges before repeating an experiment, ten times), together with velocity measurements at 43 locations. The sampling frequency of the instruments during these experiments was 128 Hz. The present study considered both the three bichromatic conditions of the GLOBEX experiments (Test Series B) and the three random wave conditions (Test Series A), whose characteristics are summarized in Table 1. Series B1 and B2 differ by their group period, while Series B2 and B3 differ by their amplitude modulation. Series A1 and A2 correspond, respectively, to intermediate and high energy sea wave conditions, while Series A3 represents a narrow-banded swell condition.

Table 1. Characteristics of GLOBEX Test Series B (bichromatic wave conditions) and A (random wave conditions). Offshore amplitudes and frequencies of the two short-wave trains for Test Series B are, respectively, a_1 and a_2, and f_1 and f_2, while T_p is the short-wave peak period and T_g is the group period. For Test Series A, the offshore wave amplitude a_1 corresponds to $H_s/2$, while γ_j denotes the JONSWAP peak enhancement factor.

Series	a_1 (m)	a_2 (m)	f_1 (Hz)	f_2 (Hz)	T_p (s)	T_g (s)	Remark
B1	0.09	0.01	0.40	0.467	2.308	15	–
B2	0.09	0.01	0.42	0.462	2.268	23.81	–
B3	0.07	0.03	0.42	0.462	2.268	23.81	–
A1	0.05	–	–	–	1.60	–	$\gamma_j = 3.3$
A2	0.10	–	–	–	2.25	–	$\gamma_j = 3.3$
A3	0.05	–	–	–	2.25	–	$\gamma_j = 20$

3.2. Data Processing

To obtain the phase lag between the infragravity wave and the short-wave group for the laboratory data, firstly the short-wave group envelope A is determined as:

$$A(t) = |\ \eta_{hf}(t) + Im(\Gamma\{\eta_{hf}\})\ |_{lf} \tag{18}$$

where η indicates the surface elevation, lf and hf denotes, respectively, low-pass and high-pass filtered (the cut-off frequency between both being set to $f_p/2$), Im indicates the imaginary part, and $\Gamma\{\}$ denotes the Hilbert transform operator. The infragravity-wave signals are obtained by low-pass filtering of the surface elevation and cross-shore velocity time series. To subsequently extract the surface elevation time series of only the shoreward propagating infragravity wave, collocated pressure and cross-shore velocity time series are used following the time-domain approach of [26], while assuming shallow water and cross-shore propagation:

$$\eta_{lf}^{\pm} = \frac{\eta_{lf} \pm u_{lf}\sqrt{h/g}}{2} \tag{19}$$

where h is the water depth corrected for sensor height above the bed, and u_{lf} is the low-pass filtered cross-shore velocity. From here, two different methods are used to obtain the phase lag from either bichromatic or random wave conditions.

For the bichromatic conditions, the correlations (r) and corresponding time lags (τ) between the incoming infragravity wave and the squared short-wave envelope are calculated following:

$$r(\tau) = \frac{\overline{\eta_{lf}^{+}(t)A^2(t+\tau)}}{\sigma_{\eta_{lf}^{+}}\sigma_{A^2}} \tag{20}$$

where $\sigma_{\eta_{lf}^{+}}$ and σ_{A^2} are, respectively, the standard deviations of η_{lf}^{+} and A^2, such that $-1 \leq r \leq 1$. The time lag at maximum negative correlation ($\tau_{max|r|}$) is then extracted, allowing to compute the so-called measured phase lag at position x as:

$$\phi_{lag}(x) = \omega_g\ \tau_{max|r|}(x) \tag{21}$$

A threshold is eventually applied on $r\left(\tau_{max|r|}\right)$ in order to only keep the phase lags corresponding to relatively high correlation values (the threshold being set to the first offshore value obtained for $r\left(\tau_{max|r|}\right)$). As expected, the phase lag measurements obtained in the surf zone are mostly discarded when applying this method.

The measured phase lags associated with the random wave conditions are computed as in de Bakker et al. [27]:

$$\phi_{lag}(f,x) = \arctan\left(\frac{Im(Cr_{A\eta_{lf}^+}(f,x))}{Re(Cr_{A\eta_{lf}^+}(f,x))}\right) \tag{22}$$

where *Re* and *Im* are the real and imaginary parts of the cross-spectrum of A and η_{lf}^+, $Cr_{A\eta_{lf}^+}$. Because this method provides a phase lag per frequency, the power spectrum of the incoming wave signal was computed (with 240 degrees of freedom) in order to select the frequency bin being the closest one to the spectral infragravity peak. The three power spectra associated with GLOBEX test Series A1 to A3 are shown in Figure 1 for a cross-shore position located in the shoaling zone. One can mainly observe on this figure the two energy peaks corresponding to the gravity band (i.e., $f > 0.2 - 0.3$ Hz) and to the IG band (i.e., $f < 0.2 - 0.3$ Hz) for each test series. Furthermore, the frequency spreading of these energy peaks is observed to be larger for Test Series A1 and A2 than for A3, according to the narrow-banded nature of the latter compared to the two others (see the corresponding JONSWAP peak enhancement factor in Table 1). More physical descriptions of these energy density spectra and the involved energy transfers are extensively discussed in de Bakker et al. [28].

Note that, due to a resampling of the time series required to compute the power spectra, the frequency bins associated with these spectra can differ from those associated with the measured phase lags, the latter being indicated by the red dashed lines on the figure. Peak frequency bins of 0.0611 Hz, 0.05 Hz and 0.0389 Hz were eventually used for Series A1, A2 and A3, respectively, which correspond to peak group periods of 16.36 s, 20 s and 25.71 s.
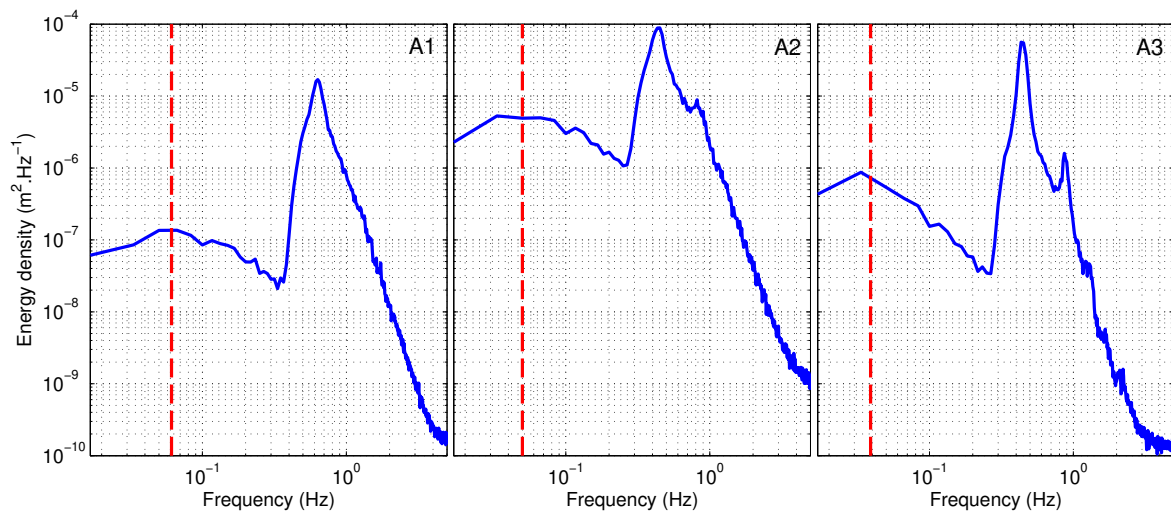

Figure 1. Energy density spectra of the incoming wave signal for GLOBEX Test Series A1, A2, and A3, at $x = 41.3$ m. Vertical dashed lines indicate the positions of the frequency bins used to perform the comparisons between observed and theoretical phase lags.

3.3. Results

Figures 2–4 show the measured phase lags for the bichromatic wave conditions B1–B3 compared with both the theoretical solution proposed in the present study (i.e., Equations (16) and (17)) and the off-resonant and near-resonant solutions of J03. The breakpoint position indicated on these three figures corresponds to the offshore limit of the breaking zone, which appeared to be a convenient choice for the fixed breakpoint location needed in our theoretical approach. We mention here that the J03 solutions were first replicated according to the bichromatic case considered in their study to ensure our correct computation of these solutions (see Appendix B). Figures 5–7 then show the comparison between measured and theoretical phase lags for the random wave conditions A1–A3, where the mean breakpoint position is indicated. Note that the discrepancy between theory and measurements

appeared to increase as the frequency bin considered for the comparison is taken increasingly away from the spectral peak (not shown). A succinct description of these results follows, before enlarging the discussion in Section 4.
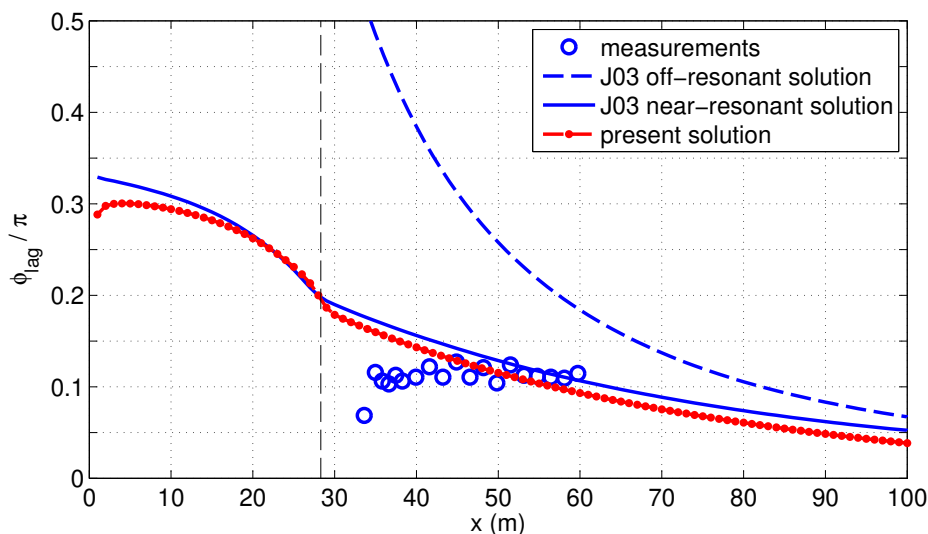

Figure 2. Theoretical versus measured phase lag for GLOBEX bichromatic conditions B1 ($T_p = 2.308$ s and $T_g = 15$ s). Breakpoint location is indicated by the vertical dashed line. (J03 refers to Janssen et al. [21].)
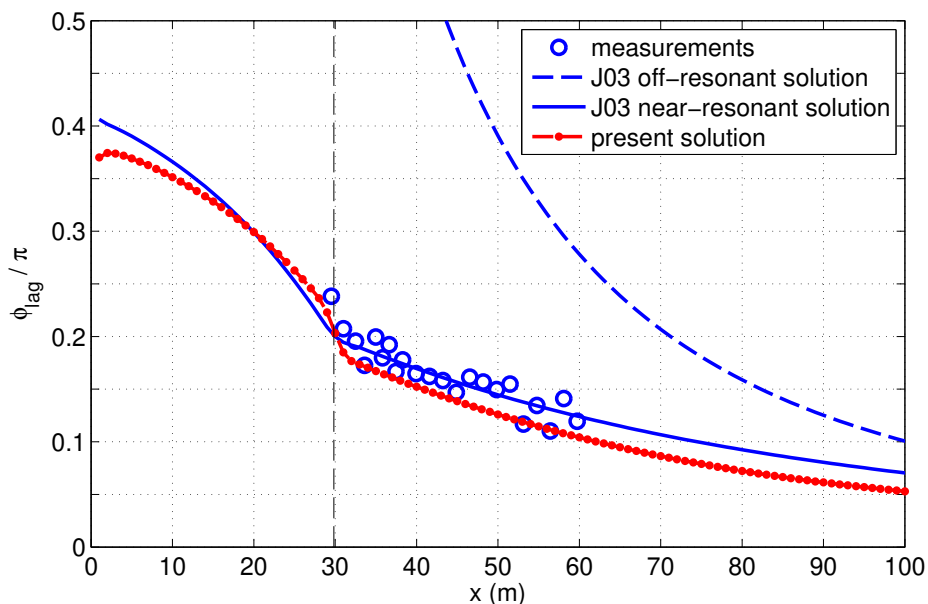

Figure 3. Theoretical versus measured phase lag for GLOBEX bichromatic conditions B2 ($T_p = 2.268$ s and $T_g = 23.81$ s). Breakpoint location is indicated by the vertical dashed line.

First, the off-resonant solution of J03 can be seen to largely overestimate the phase lag in all conditions. This confirms that, despite its relative straightforwardness to compute because of its local nature (i.e., no integration is required), this solution is not valid in shallow water, as already mentioned by J03. On the contrary, both the theoretical solution proposed in the present study and the near-resonant one of J03 appear to be in close agreement with the measurements, except for bichromatic case B1 where a plateau is observed for the distribution of data points. This unexpected behavior may be related to spurious transverse or cross-mode waves generated close to the breakpoint through resonance in the flume, which induced secondary circulations and therefore modified the mean

horizontal velocity field [29,30]. The performance skills of the two relevant solutions are synthesized in Table 2, which globally shows that the present solution yields more accurate phase lag predictions with an overall NRMSE decreasing from 18.1% to 14%, mostly due to a decrease in the overall mean bias (absolute value) from 0.045 to 0.028 rad.
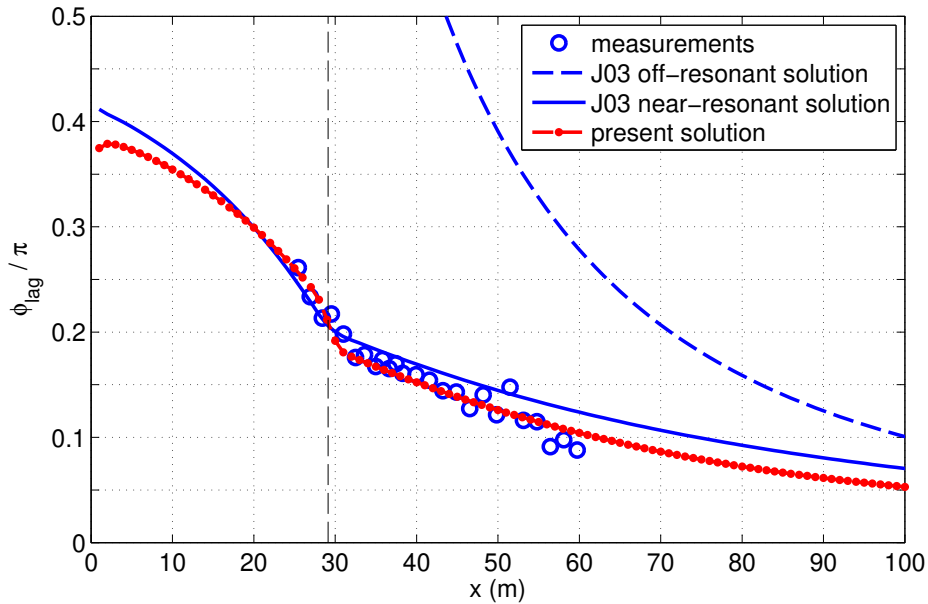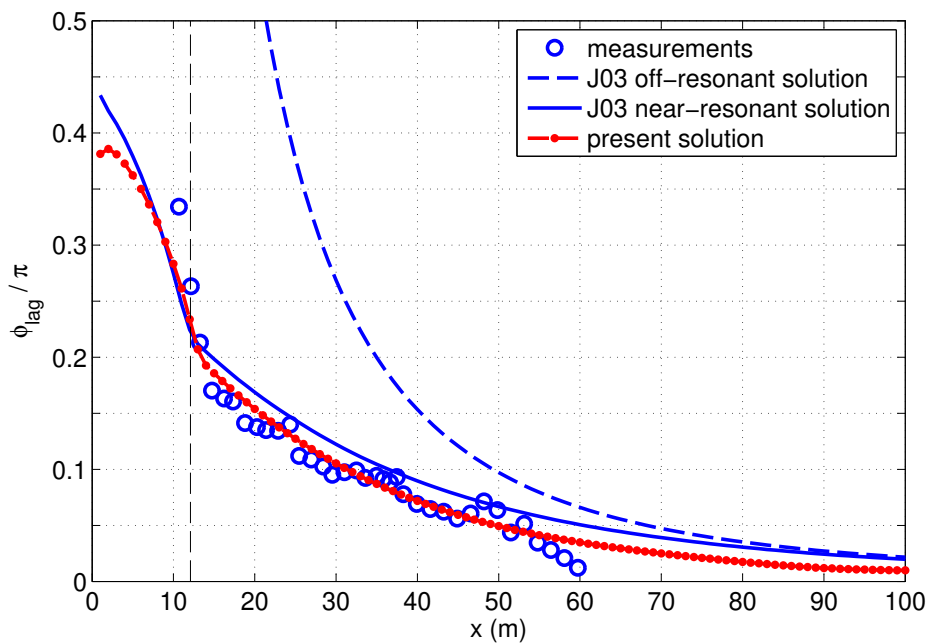

Figure 4. Theoretical versus measured phase lag for GLOBEX bichromatic conditions B3 ($T_p = 2.268$ s and $T_g = 23.81$ s). Breakpoint location is indicated by the vertical dashed line.

Figure 5. Theoretical versus measured phase lag for GLOBEX random wave conditions A1 ($T_p = 1.6$ s and a peak group period of 16.36 s was considered in this case). Breakpoint location is indicated by the vertical dashed line.
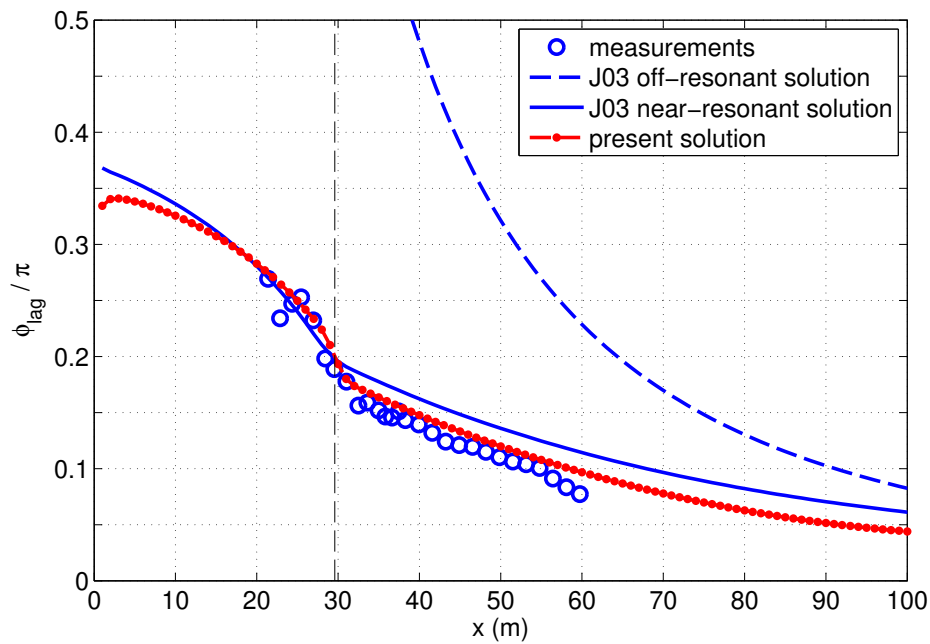
Figure 6. Theoretical versus measured phase lag for GLOBEX random wave conditions A2 ($T_p = 2.25$ s and a peak group period of 20 s was considered in this case). Breakpoint location is indicated by the vertical dashed line.
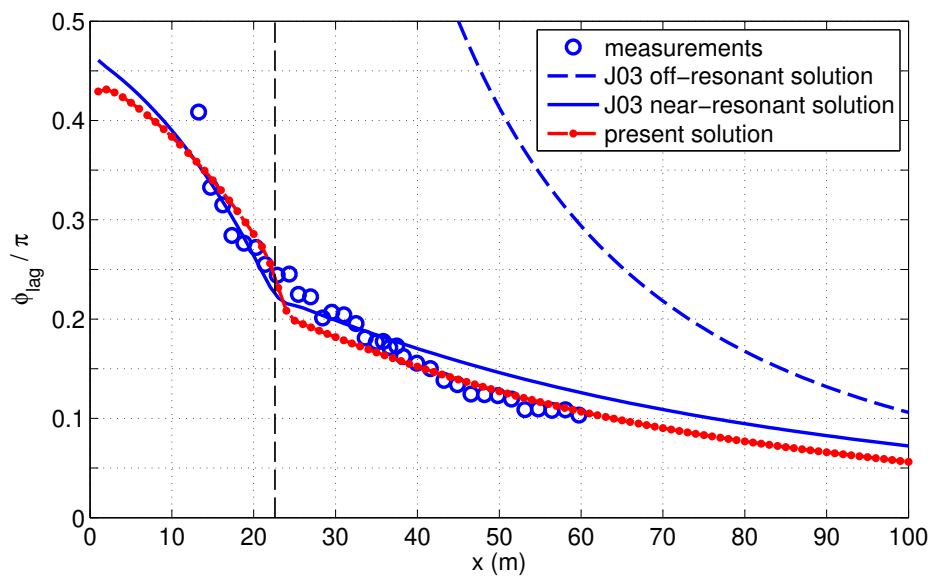

Figure 7. Theoretical versus measured phase lag for GLOBEX narrow-banded random wave conditions A3 ($T_p = 2.25$ s and a peak group period of 25.71 s was considered in this case). Breakpoint location is indicated by the vertical dashed line.

From the measurements, the phase lag is seen to be influenced by the short-wave peak period (compare A1 to A2), by the group period (compare B1 to B2), and by the amplitude modulation (or wave groupiness; compare B2 to B3). The phase lag increases with larger group period and larger short-wave peak period, but decreases with larger wave groupiness. The J03 and the presently proposed solutions do take into account the influence of both the short-wave peak period and the group period on the phase lag, but unfortunately they do not reproduce the observed effect of wave groupiness (more precisely both theoretical solutions appear to be independent of the amplitude modulation).

Eventually, the increase of the phase lag when the waves propagate towards shallower water and especially when they enter the surf zone appears to be well reproduced by both theoretical solutions.

While the high-resolution GLOBEX data allowed us to validate both our proposed theoretical solution and the near-resonant one of J03, the latter observations concerning the bound wave phase lag remain tied to the specificity of these experiments. A broader analysis of the phase lag characteristics is thus presented in Section 4, through an inter-comparison of the two relevant theoretical solutions.

Table 2. Performance of the J03 near-resonant (J03-nr) and present phase lag solutions, in terms of mean bias, root-mean-square error (RMSE) and normalized root-mean-square error (NRMSE), for GLOBEX Test Series A and B.

Series	Solution	Mean Bias (rad)	RMSE (rad)	NRMSE (%)
B1	J03-nr	0.099	0.134	38.7
	present	0.058	0.109	31.3
B2	J03-nr	−0.006	0.041	7.9
	present	−0.057	0.066	12.7
B3	J03-nr	0.037	0.057	11.4
	present	−0.006	0.033	6.6
A1	J03-nr	0.047	0.081	24.6
	present	<0.001	0.051	15.4
A2	J03-nr	0.063	0.075	15.7
	present	0.034	0.040	8.3
A3	J03-nr	0.019	0.062	10.3
	present	−0.014	0.057	9.5

4. Discussion

4.1. Theoretical Limitations

The no-reflection situation at the shoreline which is considered in the present study is a first limitation of the proposed approach. Potential effects on the phase lag of reflected IG waves propagating seaward are therefore not investigated within this framework, although it has been shown at least for the irregular wave cases that IG wave reflection at the shoreline was weak during GLOBEX [28]. The second limitation is the assumption of a fixed breakpoint position, which allowed us to avoid the generation of free waves due to the moving-breakpoint mechanism [11] and thus to focus on the bound wave only. While this assumption can be seen as over-simplistic at first sight, especially for gently sloping beaches where the breakpoint excursion is larger than for steep beaches, the narrow-banded conditions of GLOBEX Series A3 show that it can eventually be realistic since a constant location of short-wave breaking was observed in this case [28]. In fact, this assumption tends to be more realistic as the amplitude modulation of incident short-waves remains small, because of a subsequent small breakpoint excursion. In addition, the moving breakpoint mechanism is generally considered to be more important on steeper beaches [18]. As mentioned by Schäffer [12] and van Dongeren and Svendsen [17], another shortcoming of linearized models concerns the energy feedback to the short-waves, since the expected decrease (increase) of short-wave energy when it is transferred to (from) the long waves is not accounted for. Energy dissipation through infragravity-wave breaking, which has already been proposed as a dominant energy dissipation mechanism close to the shoreline [31], also adds to the list of limitations. Eventually, the frictional effects (e.g., due to bottom friction) which are not included in the present work may play a role on the infragravity wave dynamics, and therefore on the phase lag, although several studies already showed this to be minimal on sandy beaches (e.g., [32,33]) while being substantial in coral reef environments (e.g., [34,35]).

However, the close agreement between data and both theoretical solutions as seen in Section 3 suggests the above-mentioned restrictions to be of secondary importance. We therefore take the liberty

to extend the range of input conditions required to compute the bound wave phase lag in order to further analyze its characteristics in the following.

4.2. Inter-Comparison of Theoretical Solutions

The main difference between the two theoretical approaches considered in the present work is the first-order approximation in terms of depth variations on which is based the phase lag solution proposed by J03, contrary to the new one derived from the work of Schäffer [12]. More precisely, the ordering parameter, or relative bottom slope, introduced by J03 is:

$$\beta_s = \frac{h_x}{\kappa h} = \frac{h_x T_g c_g}{2\pi h} \tag{23}$$

since $\kappa = \omega_g / c_g$ in their work. The magnitude of β_s relates to the variation of the medium, which thus increases with decreasing h and with increasing h_x, T_g, and T_p (through c_g for the latter). These four parameters characterize the phase lag behavior in both theoretical approaches, which leads us to analyze their influence on the two theoretical solutions in the following.

Figure 8 shows the variation of both solutions for different values of water depth, bottom slope, group period, but a fixed peak period, while in Figure 9 the group period is fixed and the peak period is changing. The bottom slope varies from 0.01 to 0.05, and realistic values of incoming wave conditions are chosen to facilitate the interpretation of the computed phase lags: T_p ranging from 12 s to 18 s, and T_g from 100 s to 200 s. While the wave amplitude does not directly affect the phase lag (i.e., the result of Equations (16) and (17) is independent of a), it does affect the breakpoint location. An offshore wave amplitude of $a_\infty = 2$ m is eventually chosen together with a breaking index $(\gamma_b = a_b / h_b)$ of 0.4, which gives a depth at breaking of about 6.5 m. The water depths of 50 m, 20 m, and 7 m are considered in both figures to highlight the variation of the phase lag from deep water to the shoaling and the near-breaking zone.
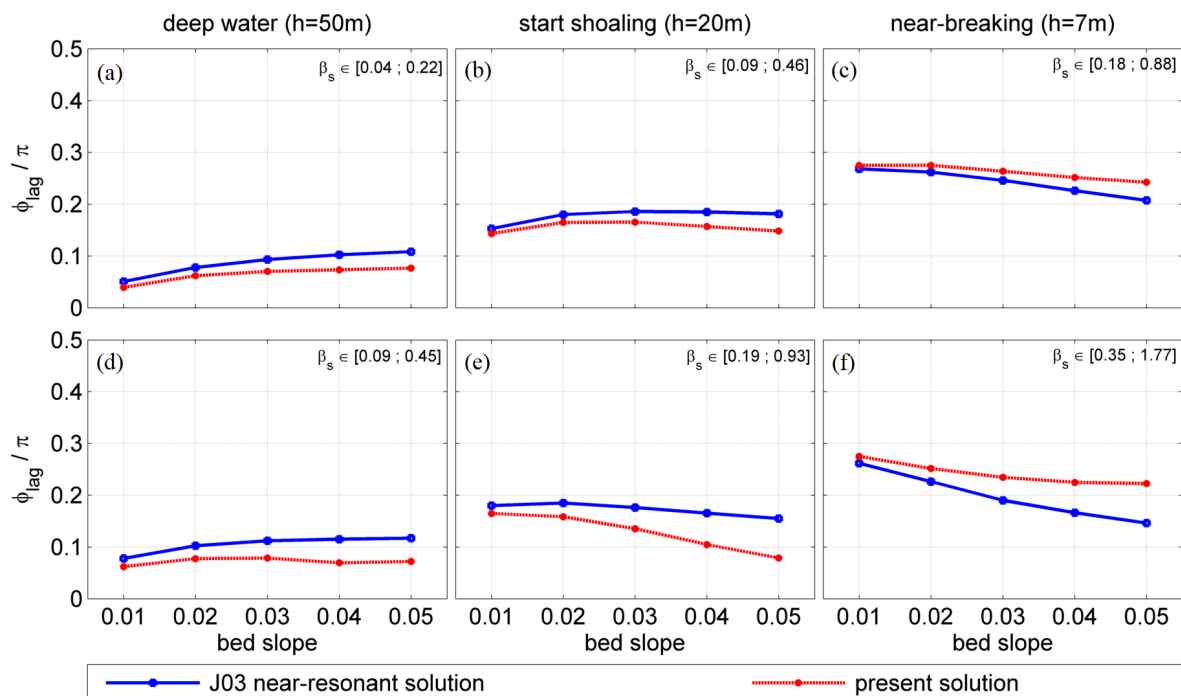

Figure 8. Inter-comparison of our proposed theoretical phase lag and J03 near-resonant one for a fixed short-wave peak period of 15 s. Subplots (**a**–**c**) correspond to $T_g = 100$ s, while subplots (**d**–**f**) correspond to $T_g = 200$ s. The range of ordering parameter β_s is indicated for each subplot.

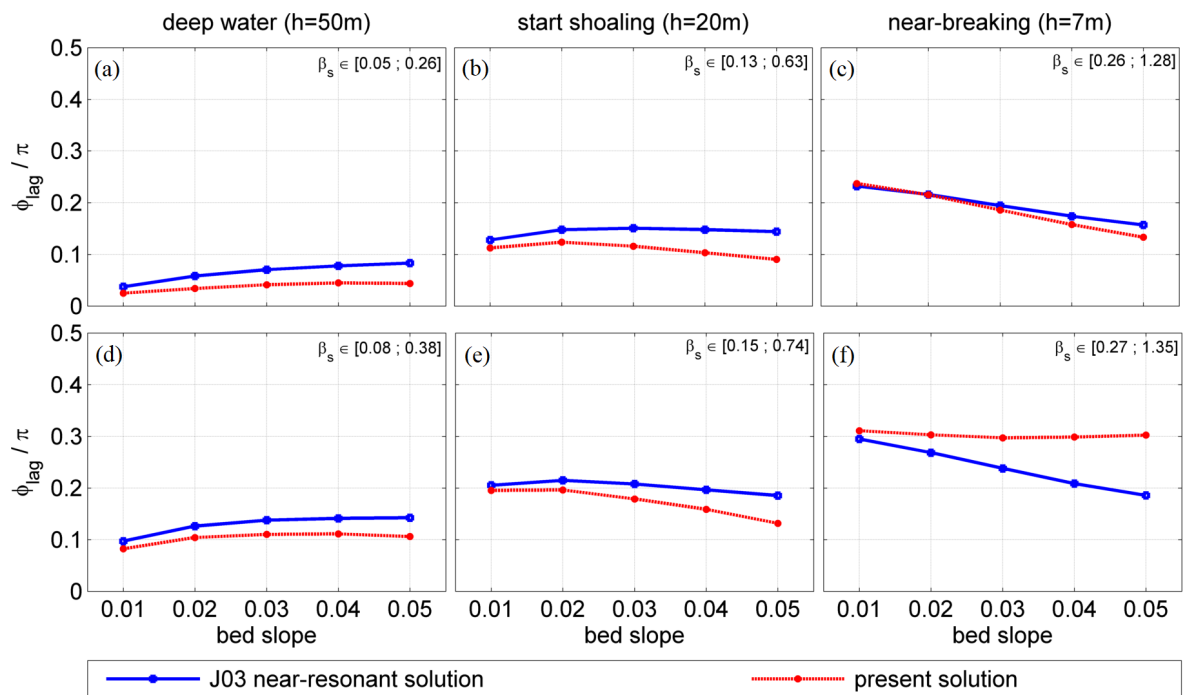**Figure 9.** Inter-comparison of our proposed theoretical phase lag and J03 near-resonant one for a fixed group period of 150 s. Subplots (**a**–**c**) correspond to $T_p = 12$ s, while subplots (**d**–**f**) correspond to $T_p = 18$ s. The range of ordering parameter β_s is indicated for each subplot.

A common feature of the bound wave phase lag is its increase as the water depth decreases, this being more pronounced for gentle slopes than steep slopes. However, at a given water depth, the phase lag does not systematically increase with decreasing bed slope, especially in deep water where the opposite relation is observed. As for the influence of peak and group periods, while increasing T_p induces a clear increase of the phase lag, interestingly, it is not always the case when T_g increases. This particular relation between the group period and the bound wave phase lag, which is not unequivocal in these results due to the additional dependence on the bed slope and the water depth, may explain the contradictory findings of Battjes et al. [18] and de Bakker et al. [27] on this point.

The discrepancy between the two solutions is seen to globally increase with the ordering parameter β_s (whose range is indicated for each subplot). This appears to be a logical consequence of the main approximation on which the approach of J03 is based, as the validity of their solution relies on a sufficiently small value of the ordering parameter (or relative bottom slope) β_s. However, one should note that the discrepancy between the two solutions is not strictly related to the magnitude of β_s, since a difference of the same magnitude between both solutions can be observed for different values of β_s. Another interesting result is the switch between the higher and lower solution when reaching the near-breaking zone (except for the case $\{T_p, T_g\} = \{12\ s, 150\ s\}$), which denotes a larger increase of the phase lag in the shoaling zone when predicted following our proposed method. However, for both approaches, the largest phase lags are predicted to appear for large short-wave peak periods in combination with gentle bed slopes and shallow water depths (see Figure 9f), while the influence of the group period remains secondary for this particular configuration (compare Figure 8c,f for a bed slope of 0.01).

Based on the above results, field sites and incident wave conditions giving relatively high values of β_s would be recommended to extensively assess the validity of both theoretical solutions in future studies.

5. Conclusions

The present work provides a new investigation of the bound wave phase lag based on the pioneer and reference work of Schäffer [12] for modeling group-forced long waves reaching the shore. The proposed semi-analytical solution for the phase lag was tested against the GLOBEX laboratory dataset [24] involving both bichromatic and random wave conditions over a gently sloping beach, together with the off-resonant and near-resonant solutions of Janssen et al. [21] (J03). Strong agreement was obtained when comparing the new solution with data for five out of six experiments, while some discrepancy appeared for one experiment (bichromatic conditions B1) due to the presence of an unexpected plateau in the data. In general, despite an occasional slight overestimation of the phase lag in the shoaling zone, these comparisons also extend the applicability of the J03 near-resonant solution to the GLOBEX dataset.

An extensive inter-comparison of our proposed phase lag solution and the one of J03 was performed to investigate in more detail their dependence on the four influencing parameters: the bed slope, the water depth, the incident short-wave peak period and the incident group period. While the bound wave phase lag is mainly seen to increase as the short-wave peak period increases and/or as the water depth decreases, the influence of both the bed slope and the group period on the phase lag is not unequivocal. Indeed, steeper bed slopes induce lower phase lags in shallow water but higher ones in deep water, while higher group periods induce higher phase lags for gentle slopes but lower ones for steep slopes. At the same time, the discrepancy between the two theoretical solutions is seen to increase as the relative bottom slope $\beta_s = h_x c_g/(\omega_g h)$ increases, in consequence to the first-order approximation in terms of β_s on which the J03 solution is based. Confronting these phase lag solutions with field data would be of great interest for future studies, provided that the field conditions do not deviate too much from the theoretical framework. In addition, it seems worthwhile also considering the phase difference between the breakpoint-forced long waves and their forcing when analyzing infragravity wave signals in coastal areas [36].

Finally, as already pointed out in several studies (e.g., [17,21,27]), the growth of IG waves in the nearshore is linked to the phase lag. The interrelated effect of the phase lag on the energy transfer from the short waves to the long waves, which causes the IG waves to grow in amplitude, is thus fundamental to thoroughly understand. While the new insights regarding the bound wave phase lag behavior presented in this work did not allow sufficiently apprehending this relation between phase lag and energy transfers, this important aspect of the IG waves dynamics will hopefully be the focus of a future study.

Abbreviations

The following abbreviations are used in this manuscript:

GLOBEX	Gently sLOping Beach EXperiments
IG	Infragravity
NRMSE	Normalized root-mean-square error
RMSE	Root-mean-square error

Appendix A. Replication of the No-Reflection Solution

In addition to the bound (long) wave, the approach of Schäffer [12] to model infragravity waves generated by incident short-wave groups over a plane sloping beach includes the main characteristics of long wave dynamics, such as their reflection at the coastline and the time-varying position of the breakpoint. However, the bound wave can be separately computed within this model, with the artifice of cancelling the long wave reflection at the coastline while considering a fixed breakpoint position (see Section 4.3.2 of his work). This so-called no-reflection solution is precisely considered in the present work since it allows directly deriving the expression for the bound wave phase lag (i.e., without the need of separating the total long wave into its incoming and outgoing components).

To ensure the correct computation of the no-reflection solution in the present work, Figure 8a of Schäffer [12] was initially replicated (see Figure A1).
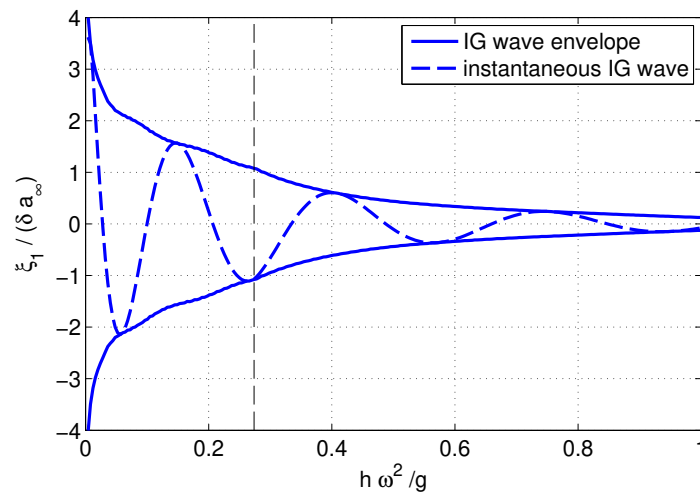

Figure A1. No-reflection solution computed according to the input parameters corresponding to Figure 8a of Schäffer [12]. In our case, $h_x = 0.01$, $T_p = 10$ s, and $T_g = 100$ s. Breakpoint location is indicated by the vertical dashed line.

Appendix B. Replication of the Off-Resonant and Near-Resonant Solutions

The bound wave phase lag solution proposed in the present work is extensively compared with the off-resonant and near-resonant solutions of Janssen et al. [21]. The correct computation of these two solutions was therefore priorly verified by replicating Figure 8a of their study (see Figure A2), which involved bichromatic wave conditions with two interacting angular frequencies of 2.8 rad·s^{-1} and 3.6 rad·s^{-1} over a bottom slope of 0.025.
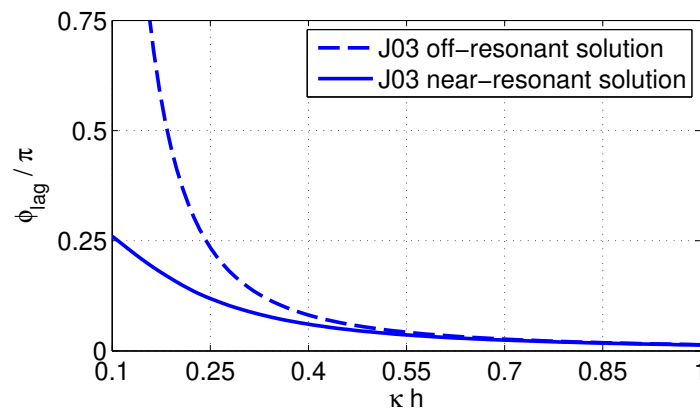
Figure A2. Phase lag computed following the off-resonant and near-resonant solutions of Janssen et al. [21], according to the conditions of their Figure 8a and as a function of κh (where $\kappa = \omega_g / c_g$).

References

1. Munk, W. Surf beat. *Trans. Am. Geophys.* **1949**, *30*, 849–854.
2. Tucker, M. Surf beats: Sea waves of 1 to 5 min. period. *Proc. R. Soc. Lond. A* **1950**, *202*, 565–573.
3. Wright, L.; Guza, R.; Short, A. Dynamics of a high-energy dissipative surf zone. *Mar. Geol.* **1982**, *45*, 41–62. [CrossRef]
4. Guza, R.; Thornton, E.B. Swash oscillations on a natural beach. *J. Geophys. Res. Ocean.* **1982**, *87*, 483–491. [CrossRef]
5. Bowers, E. Harbour resonance due to set-down beneath wave groups. *J. Fluid Mech.* **1977**, *79*, 71–92. [CrossRef]
6. Mei, C.C.; Agnon, Y. Long-period oscillations in a harbour induced by incident short waves. *J. Fluid Mech.* **1989**, *208*, 595–608. [CrossRef]
7. Wu, J.K.; Liu, P.L.F. Harbour excitations by incident wave groups. *J. Fluid Mech.* **1990**, *217*, 595–613. [CrossRef]
8. Bertin, X.; De Bakker, A.; van Dongeren, A.; Coco, G.; Andre, G.; Ardhuin, F.; Bonneton, P.; Bouchette, F.; Castelle, B.; Crawford, W.C.; et al. Infragravity waves: From driving mechanisms to impacts. *Earth Sci. Rev.* **2018**, *177*, 774–799. [CrossRef]
9. Biésel, F. Équations générales au second ordre de la houle irrégulière. *La Houille Blanche* **1952**, *3*, 372–376. [CrossRef]
10. Longuet-Higgins, M.S.; Stewart, R. Radiation stress and mass transport in gravity waves, with application to 'surf beats'. *J. Fluid Mech.* **1962**, *13*, 481–504. [CrossRef]
11. Symonds, G.; Huntley, D.A.; Bowen, A.J. Two-dimensional surf beat: Long wave generation by a time-varying breakpoint. *J. Geophys. Res. Ocean.* **1982**, *87*, 492–498. [CrossRef]
12. Schäffer, H.A. Infragravity waves induced by short-wave groups. *J. Fluid Mech.* **1993**, *247*, 551–588. [CrossRef]
13. Bowers, E. Low frequency waves in intermediate water depths. In Proceedings of the 23rd International Conference on Coastal Engineering, Venice, Italy, 4–9 October 1992; pp. 832–845.
14. Van Leeuwen, P. Low Frequency Wave Generation due to Breaking Wind Waves. Ph.D. Thesis, TU Delft, Delft University of Technology, Delft, The Netherlands, 1992.
15. Mansard, E.; Barthel, V. Shoaling properties of bounded long waves. In Proceedings of the 19th International Conference on Coastal Engineering, Houston, TX, USA, 3–7 September 1984; pp. 798–814.
16. Elgar, S.; Guza, R. Observations of bispectra of shoaling surface gravity waves. *J. Fluid Mech.* **1985**, *161*, 425–448. [CrossRef]
17. Van Dongeren, A.R.; Svendsen, I.A. *Quasi 3-D Modeling of Nearshore Hydrodynamics*; Technical Report, Research Report No. CACR-97-04; Center for Applied Coastal Research, University of Delaware: Newark, DE, USA, 1997.
18. Battjes, J.; Bakkenes, H.; Janssen, T.; van Dongeren, A. Shoaling of subharmonic gravity waves. *J. Geophys. Res. Ocean.* **2004**, *109*. [CrossRef]
19. Strickland, D.; Mourou, G. Compression of amplified chirped optical pulses. *Opt. Commun.* **1985**, *55*, 447–449. [CrossRef]

20. Maine, P.; Strickland, D.; Bado, P.; Pessot, M.; Mourou, G. Generation of ultrahigh peak power pulses by chirped pulse amplification. *IEEE J. Quantum Electron.* **1988**, *24*, 398–403. [CrossRef]

21. Janssen, T.; Battjes, J.; van Dongeren, A. Long waves induced by short-wave groups over a sloping bottom. *J. Geophys. Res. Ocean.* **2003**, *108*. [CrossRef]

22. Nielsen, P. Surf beat 'shoaling'. In Proceedings of the Conference on Coastal Dynamics, Helsingor, Denmark, 12–16 June 2017; pp. 443–450.

23. Boers, M. Simulation of a surf zone with a barred beach. Report 1. Wave heights and wave breaking. In *Communications on Hydraulic and Geotechnical Engineering*; No. 1996-05; TU Delft: Delft, The Netherlands, 1996.

24. Ruessink, B.; Michallet, H.; Bonneton, P.; Mouazé, D.; Lara, J.; Silva, P.A.; Wellens, P. Globex: Wave dynamics on a gently sloping laboraty beach. *Proc. Coast. Dyn.* **2013**, *2013*, 1351–1362.

25. Abramowitz, M.; Stegun, I.A. *Handbook of Mathematical Functions: With Formulas, Graphs, and Mathematical Tables*; Dover Publications: New York, NY, USA, 1972; Volume 55.

26. Guza, R.T.; Thornton, E.B.; Holman, R.A. Swash on steep and shallow beaches. In Proceedings of the 19th International Conference on Coastal Engineering, Houston, TX, USA, 3–7 September 1984; pp. 708–723.

27. De Bakker, A.; Tissier, M.; Marieu, V.; Sénéchal, N.; Ruju, A.; Lara, J.; Ruessink, B. Infragravity wave propagation and dissipation on a low-sloping laboratory beach. In Proceedings of the Conference on Coastal Dynamics, Arcachon, France, 23–26 June 2013; pp. 443–452.

28. De Bakker, A.; Herbers, T.; Smit, P.; Tissier, M.; Ruessink, B. Nonlinear infragravity–wave interactions on a gently sloping laboratory beach. *J. Phys. Oceanogr.* **2015**, *45*, 589–605. [CrossRef]

29. Michallet, H.; Ruessink, B.G.; da Rocha, M.V.L.M.; De Bakker, A.; Van Der A.D.; Ruju, A.; Silva, P.A.; Sénéchal, N.; Marieu, V.; Tissier, M.; et al. GLOBEX: Wave dynamics on a shallow sloping beach. In Proceedings of the HYDRALAB IV Joint User Meeting, Lisbon, Portugal, 2–4 July 2014.

30. Tissier, M.; Bonneton, P.; Michallet, H.; Ruessink, B. Infragravity-wave modulation of short-wave celerity in the surf zone. *J. Geophys. Res. Ocean.* **2015**, *120*, 6799–6814. [CrossRef]

31. De Bakker, A.; Tissier, M.; Ruessink, B. Shoreline dissipation of infragravity waves. *Cont. Shelf Res.* **2014**, *72*, 73–82. [CrossRef]

32. Thomson, J.; Elgar, S.; Raubenheimer, B.; Herbers, T.; Guza, R. Tidal modulation of infragravity waves via nonlinear energy losses in the surfzone. *Geophys. Res. Lett.* **2006**, *33*. [CrossRef]

33. Van Dongeren, A.; Battjes, J.; Janssen, T.; Van Noorloos, J.; Steenhauer, K.; Steenbergen, G.; Reniers, A. Shoaling and shoreline dissipation of low-frequency waves. *J. Geophys. Res. Ocean.* **2007**, *112*. [CrossRef]

34. Pomeroy, A.; Lowe, R.; Symonds, G.; van Dongeren, A.; Moore, C. The dynamics of infragravity wave transformation over a fringing reef. *J. Geophys. Res. Ocean.* **2012**, *117*. [CrossRef]

35. Van Dongeren, A.; Lowe, R.; Pomeroy, A.; Trang, D.M.; Roelvink, D.; Symonds, G.; Ranasinghe, R. Numerical modeling of low-frequency wave dynamics over a fringing coral reef. *Coast. Eng.* **2013**, *73*, 178–190. [CrossRef]

36. Contardo, S.; Symonds, G.; Dufois, F. Breakpoint forcing revisited: Phase between forcing and response. *J. Geophys. Res. Ocean.* **2018**, *123*, 1354–1363. [CrossRef]